Thermal Characteristics of Bioconvective Flow of a Shear-thinning Fluid Conveying Nanoparticles and Gyrotactic Cells within a Stratified Region

TOSIN OREYENI[1], ANSELM O. OYEM[2,3], BASMA SOUAYEH[4], FELIX O. OKUNLOLA[5]
[1]Department of Physical Sciences,
Precious Cornerstone University, Ibadan,
NIGERIA

[2]Department of Mathematics,
Federal University Lokoja,
NIGERIA

[3]Department of Mathematics,
Busitema University,
UGANDA

[4]Department of Physics,
King Faisal University,
SAUDI ARABIA

[5]Department of Natural Sciences,
Precious Cornerstone University, Ibadan,
NIGERIA

**Corresponding Author*

Abstract: - Thermal stratification in solar thermal systems is important for energy extraction and storage, as well as for improving the efficiency and utilization of the trapped heat energy, leading to better economic feasibility for renewable energy sources. The significance of triple stratification with the Cattaneo-Christov model in the bio-convective nanoparticles flow of thixotropic fluid coexisting with gyrotactic microorganisms is presented in this study. The incorporation of the Cattaneo-Christov heat and mass flux into the fluid model allows for a more precise prediction of heat and mass phenomena in the fluid system. The governing partial differential equations describing fluid flow are parametrized to produce a system of ordinary differential equations. Using the Optimal Homotopy Analysis Method (OHAM), the series solutions are obtained. The effects of selected pertinent parameters on the various profiles are revealed and properly reported. It is envisioned that larger values of thermal stratification result in a decrease in temperature and concentration distribution when, $S_0 = S_z = 0.1$ and $N_b = N_t = 0.5$.

Key-Words: - Cattaneo-Christov model, Stratification, Optimal Homotopy Analysis Method, Bioconvection, Nanofluid, Renewable energy systems.

Received: June 6, 2023. Revised: November 7, 2023. Accepted: December 20, 2023. Published: December 31, 2023.

1 Introduction

Thixotropy is one of the most important phenomena in science and engineering. Some materials exhibit viscosity when their shear stress or shear rate varies with the time. When exposed to mechanical agitation, for instance, shaking, these materials are rendered less viscid. When unused, they are solid-like and thus, stand for their initial viscosity. It represents a reversible process in which the damaged structure destroys and reconstructs itself at rest. This affects industrialization and engineering applications very much. It can be noticed that this kind of viscoelastic fluid takes part in the production of paint, ink, and glue in the specified industries.

The viscous viscosity for these products is low and therefore they could easily be applied on surfaces. However, as it is sheared, it ends up as a paste that does not simply run or leak as [1] puts it. This has been very important in making paints and inks that are homogeneous throughout their surface; hence, they don't get pooled or run out. Thixotropic fluids are often employed when creating drilling muds and concrete by engineers. Drill mud is a thixotropic material, which is mainly applied to the reinforcement of the borehole against its collapse. They have the ability to retain low viscosities when pumped and circulated, meaning they flow effectively through the wellbore. However, when left standing they thicken to provide the necessary support, [2]. Understanding thixotropic behavior is important to the biomedical and pharmaceutical industries. Certain pharmaceutical formulations find it beneficial to have thixotropic properties as they help in the ease of dispensing or application during use as well as improve product stability during shelf time. This includes creams, gel, and ointment. Some thixotropic materials are used in drug delivery systems whose purpose is a slow release of active ingredients.

Thixotropy may be advantageous for some uses such as coatings, adhesives, and food processors; but it could be counterproductive for medical-related applications and structure constructs. It can pose problems in the design of structural elements, and this is exemplified by the case where a structural material exhibiting the thixotropy character, suffers a reduction in apparent viscosity with time while undergoing static loads and cyclic loads, [3]. Thixotropy can have negative effects on drug delivery systems in the biomedical industry especially in pharmaceutical formulations. Even though it is used in some formulations to improve their usability, it can also have an impact on the consistency and stability of pharmaceutical products. The viscosity and flow characteristics of hydrogels, ointments, suspensions, and emulsions, for instance, may change as a result of thixotropic behavior, which may have an impact on their functionality and therapeutic efficacy, [4]. In the biomedical sector, thorough evaluation and characterization of pharmaceutical formulations can aid in determining how thixotropy affects product performance and allow for the necessary adjustments to ensure consistent and reliable drug delivery. Analysis of boundary layer flow of thixotropic fluid under various effects has been considered in the literature. Recently, [5], presented the retardation effects of the Lorentz and Darcy-Forcheimmer forces on the boundary layer flow of a thixotropic fluid containing nanoparticles. It was observed in their findings that thixotropy characteristics reinforce the motion of nanofluid. This made [6] to examine nasal cavity mucus velocity variations using two distinct power laws and thixotropic mucus layers. The effects of thixotropy and shear-thinning through consideration of the pipe flow of organic kerosene gel for different pumping conditions were looked into by [7].

Bioconvection is the term used to describe the mass movement of microorganisms in response to environmental cues such as light, temperature gradients, or chemical gradients. It is a common phenomenon in biofilms or microbial suspensions. On the other hand, nanofluids are fluids with suspended nanoparticles that have unusual thermal and flow characteristics causing these nanofluid properties to impact greatly on the behaviour of bioconvective microorganisms thereby, resulting in a change of its thermophysical properties. Researchers have looked into the modulation of bio-convection by nanofluids which may allow for better management and manipulation of microbial populations. Fields such as nutrient cycling, distribution and transportation of microorganisms around natural water bodies, ecology, and ecosystems, and treatment of wastewater, among others have attracted many scientific researchers to bioconvection processes enhancing the efficiency of bioremediation techniques, and facilitating the removal of pollutants from water systems. In the oil and gas industry, bio-convection studies are relevant to microbial-enhanced oil recovery (MEOR) techniques by employing microorganisms to increase oil recovery from reservoirs. In so doing, optimizing MEOR strategies and predicting the movement of injected microbes within the reservoir can help, ultimately increasing oil production through an understanding of bio-convection patterns and microbial behavior.

Many authors have considered the concept of bio-convection flow together with the suspension of nanoparticles. [8], considered the implication of bio-convection on the thermal effect of cross nanofluid while, [9], analyzed the bioconvective assessment for rate type nanofluid by numerical technique and, [10], presented a numerical approach to bio-convection caused by hydromagnetic flow with nanoparticles. Furthermore, [11], examined the impact of magnetic field and activation energy on immiscible steady nanofluid moving over an elastic stretched surface containing motile gyrotactic microorganisms as, [12], discussed active and passive controls of a shear-thinning fluid containing nanoparticles and gyrotactic microorganisms while

the characteristics of bioconvective flow of Casson fluid with nanoparticles on surface with non-uniform thickness was presented by [13]. Recently, [14], presented the vertical bioconvective flow of nanofluid containing microorganisms as, [15], considered magnetohydrodynamic bioconvective Eyring-Powell fluid flow on a permeable cone and plate with activation energy and viscous dissipation of a non-Newtonian fluid.

Thermal stratification is a process of layering or separating fluids or gases based on their temperatures in a medium such as air or water. It is important in solar water heaters and thermal energy storage systems, among others. When a fluid or gas is heated, it loses density and rises whereas when a fluid or gas is cooled it sinks due to increased density. Within the medium, this creates distinct layers or strata of varying temperatures. Thermal stratification is important in natural bodies of water such as lakes and oceans because it determines the distribution of aquatic organisms and influences ecosystem dynamics. Similarly, stratification can be used in thermal energy storage systems to store and extract heat energy such as in concentrated solar power plants or district heating systems. Managing thermal stratification can lead to more efficient and cost-effective systems and processes which may result in energy savings, reduced environmental impact, and improved economic performance. Likewise, [16], investigated the significance of triple stratifications in the dynamics of a micropolar fluid using nanoparticles and exponential heat production. Their result showed that as stratification increases the temperature gradient between the surface and the free stream is reduced, which lowers both fluid velocity and temperature. By using the hottest water first, the system's efficiency is improved, [17], and similar researches on stratification were done by [18], [19], [20], while an analytical approach to examine the effects of double stratification and variable fluid properties on an upper convected Maxwell fluid chemical reaction was done by [21] and [22], discussed the impact of bioconvection flow of nanofluid over a medium, among others, [23], [24], [25], [26], [27].

From the aforementioned literature, numerous researches on the concept of bioconvection flow with various fluid models have been made however, the bioconvective flow of a thixotropic fluid with triple stratification using a Cattaneo-Christov model, and the suspension of nanoparticles have not been considered. Hence, this research looks into the flow of a thixotropic fluid under the unique effects of nanoparticles, stratifications, Lorentz force, and Cattaneo-Christov heat and mass flux. This research will support microbial enhanced oil recovery (MEOR), thermal energy storage systems, and the biomedical industry.

Focusing on the analysis of the hydromagnetic bio-convective flow of shear-thinning fluid with nanoparticles, triple stratification, and Cattaneo-Christov heat and mass flux through a mathematical model framed using partial differential equations is presented and with the application of similarity transformations, these partial differential equations are converted and parameterized into the system of ordinary differential equations and the approximate analytic solution is obtained using Homotopy Analysis Method (HAM). This study is useful in the field of microbial-enhanced oil recovery (MEOR). This process is an economical approach for the recovery of unrecovered oil which is based on injecting live microorganisms containing essential nutrients into oil reservoirs through injection wells. Hence, this research provides answers to the following questions during the investigation;

i. What effect does the magnetic parameter have on various distributions at the lowest layer of stratifications?
ii. What effect does thermal stratification pose on various profiles when Brownian motion and thermophoretic parameters are raised?
iii. What is the impact of gyrotactic parameters on the density of motile microorganism's profile?
iv. What is the significance of the study to industries and contributions to SDG 7?

2 Mathematical Formulation

Taking into account the Cattaneo-Christov heat and mass flux, stratifications, fluid properties, and bioconvective hydromagnetic flow of thixotropic fluid with nanoparticles, the motile gyrotactic microorganisms in the thixotropic fluid, swims in the direction of the concentration gradient thus, forming a bioconvection (Figure 1, Appendix). This movement of gyrotactic microorganisms within the thixotropic fluid containing nanoparticles is intended to stabilize the nanoparticles' distribution and prevent the appliance from corrosion and sedimentation. The uniform surface temperature, concentration, and gyrotactic microorganisms are introduced, and based on the assumptions mentioned above, the governing partial differential equations of the bio-convective flow, [12], [20], [28], [29], [30], [31], [32], [33], [34], [35], [36], [37], [38], is given as Eq. (1) – (5) subject to boundary condition (6) – (7), where Eq. 5 is the density of gyrotactic microorganisms:

$$\frac{\partial u}{\partial x}+\frac{\partial v}{\partial y}=0, \tag{1}$$

$$\begin{aligned}
&u\frac{\partial u}{\partial x}+v\frac{\partial u}{\partial y}\\
&=\frac{\mu(T)}{\rho_f}\frac{\partial^2 u}{\partial y^2}-\frac{6R_1}{\rho_f}\left(\frac{\partial u}{\partial y}\right)^2\frac{\partial^2 u}{\partial y^2}-\frac{\mu(T)}{\rho_f}\frac{1}{k}u\\
&+(1-C_\infty)\rho_f g\beta(T-T_\infty)-g\beta^*(\rho_p-\rho_f)(C-C_\infty)\\
&+(N-N_\infty)g\gamma(\rho_{\mathrm{m}}-\rho_f)\\
&+\frac{4R_2}{\rho_f}\left[\begin{array}{c}\left(\frac{\partial u}{\partial y}\right)\left(\frac{\partial^2 u}{\partial y^2}\right)\left(u\frac{\partial^2 u}{\partial x\partial y}+v\frac{\partial^2 u}{\partial y^2}\right)\\+\left(\frac{\partial u}{\partial y}\right)^2\left(u\frac{\partial^3 u}{\partial x\partial y^2}+v\frac{\partial^3 u}{\partial y^3}+\frac{\partial u}{\partial y}\frac{\partial^2 u}{\partial x\partial y}+\frac{\partial v}{\partial y}\frac{\partial^2 u}{\partial y^2}\right)\end{array}\right]\\
&-\frac{\sigma {B_o}^2 u}{\rho_f},
\end{aligned} \tag{2}$$

$$\begin{aligned}
&u\frac{\partial T}{\partial x}+v\frac{\partial T}{\partial y}\\
&+\lambda_1\left(u^2\frac{\partial^2 T}{\partial x^2}+v^2\frac{\partial^2 T}{\partial y^2}+2uv\frac{\partial^2 T}{\partial y\partial x}+u\frac{\partial u}{\partial x}\frac{\partial T}{\partial x}+u\frac{\partial v}{\partial x}\frac{\partial T}{\partial y}\right.\\
&\left.+v\frac{\partial u}{\partial y}\frac{\partial T}{\partial x}+v\frac{\partial v}{\partial y}\frac{\partial T}{\partial y}\right)\\
&=\frac{k}{\rho C_p}\frac{\partial^2 T}{\partial y^2}+\tau\left(D_B\left(\frac{\partial T}{\partial y}\frac{\partial C}{\partial y}\right)+\frac{D_T}{T_\infty}\left(\frac{\partial T}{\partial y}\right)^2\right)\\
&+\frac{Q_o}{(\rho C_p)_f}e^{-y\sqrt{\frac{\alpha}{\vartheta_f}}};
\end{aligned} \tag{3}$$

$$\begin{aligned}
&\frac{\partial C}{\partial x}+v\frac{\partial C}{\partial y}\\
&+\lambda_2\left(u^2\frac{\partial^2 C}{\partial x^2}+v^2\frac{\partial^2 C}{\partial y^2}+2uv\frac{\partial^2 C}{\partial y\partial x}+u\frac{\partial u}{\partial x}\frac{\partial C}{\partial x}+u\frac{\partial v}{\partial x}\frac{\partial C}{\partial y}\right.\\
&\left.+v\frac{\partial u}{\partial y}\frac{\partial C}{\partial x}+v\frac{\partial v}{\partial y}\frac{\partial C}{\partial y}\right)\\
&=D_B\left(\frac{\partial^2 C}{\partial y^2}\right)\\
&+\frac{D_T}{T_\infty}\left(\frac{\partial^2 T}{\partial y^2}\right),
\end{aligned} \tag{4}$$

$$u\frac{\partial N}{\partial x}+v\frac{\partial N}{\partial y}+\frac{bW_c}{(C_w-C_\infty)}\left[\frac{\partial}{\partial y}\left(N\frac{\partial C}{\partial y}\right)\right]=D_n\frac{\partial^2 N}{\partial y^2}, \tag{5}$$

subjected to the boundary conditions;

$$u=ax,\quad v=0,\quad T=T_w,\quad C-C_w,\quad N=N_w \text{ at } y=0, \tag{6}$$

$$u\to 0,\quad T\to T_\infty,\quad C\to C_\infty,\quad N\to N_\infty \text{ as } y\to\infty. \tag{7}$$

Where, u and v are velocity components along x and y directions respectively, $\tau=\frac{(\rho c)_p}{(\rho c)_f}$ is the ratio of heat capacity of nanoparticle material to heat capacity of base fluid, μ_f is dynamic viscosity, ρ_f is density of base fluid, N is motile microorganism concentration, α is thermal diffusivity, c_p is specific heat capacity,σ_f is electrical conductivity, B_0 is strength of uniform magnetic field, T, C, N are temperature, nanoparticle concentration, microorganism concentration within the boundary layer, T_∞, C_∞, N_∞ are temperature, nanoparticle concentration, microorganism concentration of ambient fluid, g is acceleration due to gravity, β, β^*, γ are thermal, solutal and motile microorganism expansion coefficient, k_f is thermal conductivity of base fluid, D_B is Brownian diffusion coefficient, D_T is thermophoresis diffusion coefficient, D_n is microorganism diffusion coefficient, Q_0 is volumetric heat generation coefficient, b is chemotaxis constant, λ_1 and λ_2 are the relaxation time for heat and mass flux, respectively.

The suitable similarity transformation used is,

$$\begin{aligned}
\eta=y\left(\frac{a^{\frac{1}{2}}}{\vartheta^{\frac{1}{2}}}\right),\psi(x,y)=f(\eta)\left(a^{\frac{1}{2}}\vartheta^{\frac{1}{2}}\right)x,\\
\theta(\eta)=\frac{T-T_\infty}{(T_w-T_0)}=\frac{T-T_\infty}{m_1x},\\
\phi(\eta)=\frac{C-C_\infty}{(C_w-C_0)}=\frac{C-C_\infty}{m_3x},\\
\omega(\eta)=\frac{N-N_\infty}{(N_w-N_0)}=\frac{N-N_\infty}{m_5x}.
\end{aligned} \tag{8}$$

The model of temperature dependent viscosity obtained from Batchelor's experimental data is of the form

$$\mu(T)=\mu^*[1+b(T_w-T). \tag{9}$$

To make the inclusion of stratification in the fluid model clear, the thermal stratification at the wall (T_w), solutal stratification at the wall (Cw), motile microorganisms at the wall (N_w) and the free stream.$(T_\infty, C_\infty, N_\infty)$ are defined as:

$$T_w=T_0+m_1x,\qquad T_\infty=T_0+m_2x, \tag{10}$$

$$C_w=C_0+m_3x,\qquad C_\infty=C_0+m_4x, \tag{11}$$

$$N_w=N_0+m_5x,\qquad N_\infty=N_0+m_6x, \tag{12}$$

where, T_0, C_0 and N_0 are the reference temperature, nanoparticles concentration, and motile micro-organisms' concentration respectively, and (m_1, m_2), (m_3, m_4) and (m_5, m_6) are the temperature, nanoparticles concentration, and motile microorganisms' concentration coefficients respectively.

Introducing the stream function $\psi(x,y)$ and other similarity variables, Eq. (1) is satisfied automatically and Eqs. $(2)-(5)$ with the boundary conditions $(6)-(7)$ becomes;

$$[1+(1-\theta)\xi\frac{d^3f}{d\eta^3}-\left(\frac{df}{d\eta}\right)^2+f(\eta)\frac{d^2f}{d\eta^2}-\xi\frac{d^2f}{d\eta^2}\frac{d\theta}{d\eta}+K_1\left(\frac{d^2f}{d\eta^2}\right)^2\frac{d^3f}{d\eta^3}-M\frac{df}{d\eta}+\mathrm{R_b}w+G_r\theta-N_r-[1+(1-\theta)\xi]P_s\frac{df}{d\eta}+K_2\left[\frac{df}{d\eta}\left(\frac{d^2f}{d\eta^2}\right)^2\frac{d^3f}{d\eta^3}-f\frac{d^2f}{d\eta^2}\left(\frac{d^3f}{d\eta^3}\right)^2-f\left(\frac{d^2f}{d\eta^2}\right)^2\frac{d^4f}{d\eta^4}+\left(\frac{d^2f}{d\eta^2}\right)^4\right]=0, \quad (13)$$

$$\frac{d^2\theta}{d\eta^2}+\mathrm{P_r}N_b\frac{d\phi}{d\eta}\frac{d\theta}{d\eta}+\mathrm{P_r}N_t\left(\frac{d\theta}{d\eta}\right)^2-\mathrm{P_r}\frac{df}{d\eta}(S_t+\theta)+\mathrm{P_r}f(\eta)\frac{d\theta}{d\eta}-\mathrm{P_r}\delta_t\left(\frac{df}{d\eta}\frac{df}{d\eta}(S_t+\theta)+f^2\frac{d^2\theta}{d\eta^2}-f\frac{df}{d\eta}\frac{d\theta}{d\eta}-f\frac{d^2f}{d\eta^2}(S_t+\theta)\right)+\mathrm{P_r}\lambda e^{-\eta}=0, \quad (14)$$

$$\frac{d^2\phi}{d\eta^2}-L_e\frac{df}{d\eta}(S_o+\phi)+L_ef(\eta)\frac{d\phi}{d\eta}-L_e\delta_n\left(f^2\frac{d^2\phi}{d\eta^2}-f(\eta)\frac{df}{d\eta}\frac{d\phi}{d\eta}+\frac{df}{d\eta}\frac{df}{d\eta}(S_o+\phi)-f\frac{d^2f}{d\eta^2}(S_o+\phi)\right)+\frac{N_t}{N_b}\frac{d^2\theta}{d\eta^2}=0, \quad (15)$$

$$\frac{d^2\omega}{d\eta^2}-S_{cm}\frac{df}{d\eta}(S_z+\omega)+S_{cm}f(\eta)\frac{d\omega}{d\eta}-P_e\left(\omega\frac{d^2\phi}{d\eta^2}+\frac{d\phi}{d\eta}\frac{d\omega}{d\eta}+\varsigma\frac{d^2\phi}{d\eta^2}+S_z\frac{d^2\phi}{d\eta^2}\right)=0, \quad (16)$$

subject to the dimensionless boundary conditions

$$\frac{df}{d\eta}(0)=1,\quad f(0)=0,\quad \theta(0)=1-S_t,\phi=1-S_o\omega(0)=1-S_z \quad (17)$$

$$f'(\infty)\to 0,\qquad \theta(\infty)\to 0,\quad \phi(\infty)\to 0,\quad \omega(\infty)\to 0. \quad (18)$$

Where the governing dimensionless parameters;

$$M=\frac{\sigma_f B_o^2}{a\rho_f},\quad G_r=\frac{g\beta(1-C_\infty)(T_w-T_0)}{\rho_f a^2 x},\quad N_r=\frac{g(C_w-C_0)(\rho_p-\rho_f)}{\rho_f a^2 x},\quad Pr=\frac{\vartheta_f}{\alpha_f},$$

$$R_b=\frac{g\gamma(\rho_m-\rho_f)(N_w-N_0)}{\rho_f a^2 x},\quad N_t=\frac{(\rho C_p)_f}{\vartheta_f(\rho C_p)_f}\frac{D_T}{T_\infty}(T_w-T_0),\quad N_b=\frac{(\rho C_p)_f}{\vartheta_f(\rho C_p)_f}D_B(C_w-C_0),$$

$$L_e=\frac{\vartheta_f}{D_B},\quad S_{cm}=\frac{\vartheta_f}{D_n},\quad P_e=\frac{bW_c}{D_n}\quad \lambda=\frac{Q_o}{a(\rho C_p)_f},\quad K_1=-\frac{6R_1a^3x^2}{\rho_f\vartheta^2},\quad K_2=\frac{4R_2a^4x^2}{\rho_f\vartheta^2},\quad \delta_t=\lambda_1 a,$$

$$\delta_n=\lambda_2 a,\quad \varsigma=\frac{N_0}{(N_w-N_0)},\quad S_t=\frac{m_2}{m_1},\quad S_o=\frac{m_4}{m_3},\quad S_z=\frac{m_6}{m_5}, \quad (19)$$

are the magnetic parameter, modified local Grashof number, Buoyancy ratio parameter, Prandtl number, bio-convection Rayleigh number, micropolar parameter, thermophoresis parameter, Brownian motion parameter, Lewis number, Schmidt number for diffusing motile microorganisms, Peclet number, space-dependent internal heat source parameter, thixotropic parameters, relaxation time parameter due to heat flux, relaxation time parameter due to mass flux, gyrotactic microorganisms concentration difference parameter, thermal stratification parameter, solutal stratification parameter, gyrotactic microorganism density stratification parameter respectively.

3 Method of Solution

Without solving the given nonlinear partial differential problem Eq. (1) – (5) subject to boundary conditions (6) – (7), it is required to determine what types of base functions are appropriate to represent the solution; first by examining the physical context and the initial/boundary conditions of the nonlinear differential problem. Given the dimensionless boundary conditions (17) and (18), $f(\eta)$, $\theta(\eta)$, $\phi(\eta)$ and $\omega(\eta)$ can be expressed by setting the base functions to be:

$$\langle \eta^j \exp(-n j) \mid j\geq 0, n\geq 0\rangle. \quad (20)$$

The solutions for $f(\eta)$ and $\theta(\eta)$ can be represented in series form as:

$$f(\eta)=a_{0,0}^0+\sum_{n=0}^{\infty}\sum_{k=0}^{\infty}a_{n,k}^k\,\eta^k\exp(-nj) \quad (21)$$

$$\theta(\eta) = \sum_{n=0}^{\infty}\sum_{k=0}^{\infty} b_{n,k}^{k}\,\eta^{k}\exp(-nj) \tag{22}$$

$$\phi(\eta) = \sum_{n=0}^{\infty}\sum_{k=0}^{\infty} c_{n,k}^{k}\,\eta^{k}\exp(-nj) \tag{23}$$

$$\omega(\eta) = \sum_{n=0}^{\infty}\sum_{k=0}^{\infty} d_{n,k}^{k}\,\eta^{k}\exp(-nj). \tag{24}$$

where $a_{n,k}^{k}$, $b_{n,k}^{k}$, $c_{n,k}^{k}$ and $d_{n,k}^{k}$ are the coefficients. As long as such a set of base functions are determined, the auxiliary function $H(\eta)$, the initial approximations $f_o(\eta), \theta_o(\eta), \phi_o(\eta)$ and $\omega(\eta)$ and the auxiliary linear operators L_f, L_θ, L_ϕ and L_ω are selected in such a way that all solutions exist and are expressed by these sets of base functions. Therefore, in framing the Optimal Homotopy Analysis Method (OHAM), the rule of solution expressions in choosing the auxiliary function $H(\eta)$, the initial approximation $f_o(\eta), \theta_o(\eta), \phi_o(\eta)$ and $\omega_o(\eta)$ is applied to Eqs. (14) – (16) together with the dimensionless conditions (17) and (18) and expressed as:

$$f_o(\eta) = 1 - e^{-\eta},\ \theta_o(\eta) = 1 - S_t e^{-\eta},$$
$$\phi_o(\eta) = 1 - S_o e^{-\eta},\ \omega_o(\eta) = 1 - S_z e^{-\eta} \tag{25}$$

Let the Linear operators L_f, L_θ, L_ϕ and L_ω are:

$$L_f[f(\eta;q)] = \frac{\partial^4 f(\eta;q)}{\partial\eta^4} - \frac{\partial f(\eta;q)}{\partial\eta} \tag{26}$$

$$L_\theta[\theta(\eta;q)] = \frac{\partial^2\theta(\eta;q)}{\partial\eta^2} - \theta(\eta;q) \tag{27}$$

$$L_\phi[\phi(\eta;q)] = \frac{\partial^2\phi(\eta;q)}{\partial\eta^2} - \phi(\eta;q) \tag{28}$$

$$L_\omega[\omega(\eta;q)] = \frac{\partial^2\omega(\eta;q)}{\partial\eta^2} - \omega(\eta;q) \tag{29}$$

The operators L_f, L_θ, L_ϕ and L_ω have the following properties;

$$L_f[C_1 + C_2 e^{-\eta} + C_3 e^{-\eta}] = 0,$$
$$L_\theta[C_4 e^{-\eta} + C_5] = 0,$$
$$L_\phi[C_6 e^{-\eta} + C_7] = 0,$$
$$L_\omega[C_8 e^{-\eta} + C_9] = 0, \tag{30}$$

where, $C_1, C_2, C_3, C_4, C_5, C_6, C_7, C_8, C_9$ are constants and the linear operators are solved using Wolfram Mathematica.

The simulations for different values of the controlling parameters were conducted using the approximate analytical method described in the preceding sections. The effects of various embedded physical factors on the flow will be covered in the following section. In the analysis, the chosen values for the selected parameters are; $M = 0.5, N_b = N_t = 0.5, \xi = 0.3, K_1 = K_2 = 0.1, S_t = S_o = S_z = 0.3, \lambda = 0.4, P_s = 0.2, P_r = 0.7, L_e = S_c = 1.0, G_r = N_r = R_b = 0.5, P_e = 0.5,\ \delta_n = \delta_t = 0.1.$

Table 1 (Appendix) displays the numerical values of skin friction coefficients $-f''(0)$ and reduced Nusselt number $-\theta'(0)$ for various values of N_b. It is observed that coefficient of skin friction is raised for the first two entries of N_b and later diminishes for the last two entries of N_b, and reduced Nusselt number declines for all the entries of N_b. Table 2 (Appendix) shows the numerical values of the skin friction coefficients $-f''(0)$ and reduced Nusselt number $-\theta'(0)$ for various values of N_t. It is observed that skin friction coefficient increases for the first two and the last two entries of N_t while reduced Nusselt number increases for all values of N_t.

Figure 2 (Appendix) reveals the impact of non-Newtonian parameters K_1 and K_2 on the velocity distribution when $S_t = S_o = S_z = 0.1$ and $N_b = N_t = 0.5$. It is noticed that incremental values of K_1 and K_2 results in a rise in the velocity profiles. At the lowest layer of fluid stratification (hypolimnion) and at a high value Brownian motion, there is sufficient energy to boost the velocity of the fluid and associated boundary layer thickness. While on the contrary, temperature and concentration of nanoparticles decreases with increasing values of K_1 and K_2 in Figure 3 and Figure 4 in Appendix.

Figure 5 (Appendix) displays the impact of magnetic parameter M on the velocity distribution with $S_t = S_o = S_z = 0.1$ and $N_b = N_t = 0.5$. For higher values of M, it is observed that velocity profiles decline and this trend is due to the fact that Lorentz force arises from the interaction between a charged particle and, both electric and magnetic field which poses influence on the velocity profiles of the fluid flows. When magnetic fields are present, it has the power to change the velocity profiles of fluids hence, incremental values of M correspond to significant increase in the profiles of temperature, concentration of nanoparticles and density of motile gyrotactic micro-organisms respectively as displayed in Figure 6, Figure 7 and Figure 8 in Appendix**.** This observation is as result of the fact that when an electrically conducting fluid flows through a magnetic field, the Lorentz force plays a role of a drag-like force, generating electrical currents within the fluid. The electric currents generated, leads to dissipation of energy in the form of heat and thereafter, result in localized temperature increase at the boundaries of fluid.

The effect of thermal stratification S_t is revealed in Figure 9 and Figure 10 in Appendix. It is obvious from these figures that increasing values of S_t lead to diminution of temperature and concentration of nanoparticles profiles when $S_o = S_z = 0.1$ and $N_b = N_t = 0.5$. This reaction is attributed to the fact that S_t influences the heat transfer characteristics of the fluid. In Figure 11 and Figure 12 in Appendix, the influence of solutal stratification parameter S_o on temperature and concentration of nanoparticles profiles are displayed. It is observed that S_o is a decreasing function of both temperature and concentration of nanoparticles profiles. That is, when there is strong solutal stratification, there is a corresponding reduction in the convective heat transfer between different fluid layers which leads to decrease in temperature profiles. Likewise, when solutal stratification is strong, diffusion process becomes more prominent and intensifies as solute particles tend to redistribute themselves hence, reducing the concentration difference between regions.

In Figure 13 and Figure 14 in Appendix, the contribution of thermal relaxation parameter δ_t on various profiles is presented. From Figure 13 (Appendix), it is noticed that temperature profile diminishes with augmenting values of the thermal relaxation parameter δ_t this is due to the fact that a larger relaxation parameter implies that the system can reach a state of equilibrium more quickly. An enhancement in the concentration of nanoparticles profiles for larger values of δ_t is envisioned in Figure 14 (Appendix). The escalation of solutal relaxation parameter δ_n leads to diminution of the temperature profile as observed in Figure 15 (Appendix) and incremental values of solutal relaxation parameter δ_n causes a noticeable decline in concentration of nanoparticles profiles when $N_t = N_b = 0.5$ in Figure 16 (Appendix) while, Figure 17 (Appendix) depicts that a conspicuous decline is noticed in density of the motile microorganism profile when gyrotactic microorganism's parameter ς is raised.

3.1 Convergence of the OHAM

The interval on $\hbar$-curve becomes parallel to the $\hbar$-axis if recognized as the set of admissible values of non-zero auxiliary parameters $\hbar_f, \hbar_\theta, \hbar_\phi$ and $\hbar_\omega$ for which the solutions series converges. Figure 18, Figure 19, Figure 20 and Figure 21, in Appendix, the range of acceptable values of $\hbar_f, \hbar_\theta, \hbar_\phi$, and $\hbar_\omega$ are $-1.30 \leq \hbar_f \leq -0.60$, $-1.40 \leq \hbar_\theta \leq -0.70$, $-0.90 \leq \hbar_\phi \leq -0.60$ and $-0.85 \leq \hbar_\omega \leq -0.55$. Obviously, from the $\hbar$-curves for this problem, we obtained the approximate optimal values of $\hbar_f, \hbar_\theta, \hbar_\phi$, and $\hbar_\omega$ at $10th$- order of approximations as $-0.6619, -1.1429, -0.8590$ and -0.5774.

4 Conclusion

The impact of triple stratification on the bio-convective flow of a fluid containing tiny particles and a Cattaneo-Christov heat and mass flux has been duly considered in Eq. 13 – Eq. 16 subject to the dimensionless conditions Eq. 16 and Eq. 17. The governing dimensionless parameters in Eq. 19 together with assigned values were analytically resolved and from the obtained results, the following conclusions are made:

1. Velocity of the thixotropic fluid increases as the thixotropic parameters K_1 and K_2 are raised at the lowest layer of stratification.
2. Velocity of fluid also declines for larger values of magnetic parameter M caused as a result of the appearance of Lorentz force which arises from the interaction between charged particles and both electric and magnetic fields.
3. Convective heat transfer declines between different fluid layers as a result of the influence of strong solutal stratification parameter S_o. When the thermal relaxation parameter δ_n is increased, the fluid's temperature decreases.
4. Large values of the gyrotactic microorganism's parameter ς are predicted to result in a noticeable decline in density of the motile microorganism distribution.

For consideration of future research, the current model can be extended to hybrid and ternary hybrid nanofluids in the presence of quartic autocatalytic reaction over various geometries which has enormous applications in industries and engineering fields.

Acknowledgement:
The authors are thankful to the reviewers and editor-in-chief for their support, observation and ideas towards the improvement of this article.

References:

[1] Z. Żołek-Tryznowska, Rheology of Printing Inks, *Printing on Polymers*, 2016, pp. 87-99, https://doi.org/10.1016/B978-0-323-37468-2.00006-3

[2] A. Yahia, S. Mantellato, R.J. Flatt, *Concrete rheology, A basis for understanding chemical*

admixtures, Science and Technology of Concrete Admixtures, 2016, pp. 97-127, https://doi.org/10.1016/B978-0-08-100693-1.00007-2

[3] A. McLachlan, O. Defeo, *The interstitial environment*, *The Ecology of Sandy Shores*, (Third Edition), Academic Press, 2018, pp. 37-62, https://doi.org/10.1016/B978-0-12-809467-9.00003-5

[4] C.H. Lee, V. Moturi, Y. Lee, Thixotropic property in pharmaceutical formulations, *Journal of Controlled Release*, Vol.136, No.2, 2009, pp. 88-98, https://doi.org/10.1016/j.jconrel.2009.02.013

[5] G. Rasool, N.A. Ahammad, M.R. Ali, N.A. Shah, X. Wang, A. Shafiq, A. Wakif, Hydrothermal and mass aspects of MHD non-Darcian convective flows of radiating thixotropic nanofluids nearby a horizontal stretchable surface: Passive control strategy, *Case Studies in Thermal Engineering*, Vol.42, 2023, https://doi.org/10.1016/j.csite.2022.102654

[6] M.A. Modaresi, Numerical investigation of mucociliary clearance using power law and thixotropic mucus layers under discrete and continuous cilia motion, *Biomech Model Mechanobiol*, Vol.22, 2023, pp. 253-269, https://doi.org/10.1007/s10237-022-01645-7

[7] M.G. Li, Q.L. Cao, X. Chen, M. Massoudi, W.T. Wu, Numerical simulations of the flow of a kerosene gel: Effects of thixotropy and shear-thinning, *International Journal of Non-Linear Mechanics*, Vol.153, 2023, https://doi.org/10.1016/j.ijnonlinmec.2023.104421

[8] A.S.M. Aljaloud, L. Manai, I. Tlili, Bio-convection flow of Cross nanofluid due to cylinder with activation energy and second order slip features, *Case Studies in Thermal Engineering*, Vol.42, 2023, https://doi.org/10.1016/j.csite.2023.102767

[9] Z. Liu, S. Li, T. Sadaf, S.U. Khan, F. Alzahrani, M.I. Khan, S.M. Eldin, Numerical bio-convective assessment for rate type nanofluid influenced by Nield thermal constraints and distinct slip features, *Case Studies in Thermal Engineering*, Vol.44, 2023, https://doi.org/10.1016/j.csite.2023.102821

[10] E.A. Algehyne, M. Areshi, A. Saeed, M. Bilal, W. Kumam, P. Kumam, Numerical simulation of bio-convective Darcy Forchhemier nanofluid flow with energy transition over a permeable vertical plate, *Scientific Reports*, Vol.12, 2022, https://doi.org/10.1038/s41598-022-07254-9

[11] A. Shahid, H.L. Huang, M.M. Bhatti, M. Marin, Numerical computation of magnetized bio-convection nanofluid flow with temperature-dependent viscosity and Arrhenius kinetic, *Mathematics and Computers in Simulation*, Vol.200, 2022, pp. 377-392, https://doi.org/10.1016/j.matcom.2022.04.032

[12] O.K. Koriko, N.A. Shah, S. Saleem, J.D. Chung, A.J. Omowaye, T. Oreyeni, Exploration of bio-convection flow of MHD thixotropic nanofluid past a vertical surface coexisting with both nanoparticles and gyrotactic microorganisms. *Scientific Reports*, Vol.11, No.1, 2021, pp. 16627, https://doi.org/1038/s41598-021-96185-y

[13] M. Imran, T. Kamran, S.A. Khan, T. Muhammad, H. Waqas, Physical attributes of bio-convection in nanofluid flow through a paraboloid of revolution on horizontal surface with motile microorganisms, *International Communications in Heat and Mass Transfer*, Vol.133, 2022, https://doi.org/10.1016/j.icheatmasstransfer.2022.105947

[14] M.R. Moradi, Kh. Hosseinzadeh, A. Hasibi, D.D. Ganji, Hydrothermal study on nano-bioconvective fluid flow over a vertical plate under the effect of magnetic field. *International Journal of Computation and Methodology*, Vol.85, No. 4 2024, pp. 469-483, https://doi.org/10.1080/10407790.2023.2241632

[15] F. Peter, P. Sambath, S. Dhanasekaran, Analyzing the MHD bioconvective eyring-powell fluid flow over an upright cone/plate surface in a porous medium with activation energy and viscous dissipation, *Computation*, Vol.12, No. 3, 2024, pp. 48, https://doi.org/10.3390/compuation12030048

[16] S. Rehman, A. Anjum, M. Farooq, Hasim, M.Y. Malik, Melting heat phenomenon in thermally stratified fluid reservoirs (Powell-Eyring fluid) with Joule heating, *International Communications in Heat and Mass Transfer*, Vol.137, 2022.

[17] K. Jagan, S. Sivasankaran, Soret and Dufour and triple stratification effect on MHD flow with velocity slip towards a stretching cylinder, *Mathematical and Computational*

Applications, Vol.27, No. 2, 2022, pp. 25, https://doi.org/10.3390/mca27020025

[18] B.M. Tamilzharasan, S. Karthikeyan, M.K. Kaabar, M. Yavuz, F. Ozkose, Magneto mixed convention of Williamson Nanofluid flow through a double stratified porous medium in attendance of activation energy, *Mathematical and Computational Applications*, Vol. 27, No. 3, 2022, pp. 46.

[19] J. Zheng, T. Yu, B. Lei, R. Lv, Study on the influencing factors of thermal performance of radiant heating floor with the intensive solar irradiation, *Applied Thermal Engineering*, Vol. 232, 2023, https://doi.org/10.1016/j.applthermaleng.2023.121077

[20] M.T. Akolade, T. Akhtar, M.M. Awad, Y.O. Tijani, A.T. Adeosun, Bioconvection analysis of EMHD and dissipative Williamson nanofluid over a three dimensional riga plate with joule heating effect, *International Journal of Modelling and Simulation*, 2023, https://doi.org/10.1080/02286203.2265524

[21] S.K. Mondal, D. Pal, Computational analysis of bioconvective flow of nanofluid containing gyrotactic microorganisms over a nonlinear stretching sheet with variable viscosity using HAM, *Journal of Computational Design and Engineering*, Vol. 7, No. 2, 2020, pp. 251-267, https://doi.org/10.1093/jcde/qwaa021

[22] W.A. Khan *et al.,* Impact of stratification phenomena on a nonlinear radiative flow of sutterby nanofluid, *Journal of Materials Research and Technology*, Vol.15, 2021, pp. 306-314.

[23] S.B. Chen *et al.,* Thermophoretic particle deposition in the flow of dual stratified Casson fluid with magnetic dipole and generalized Fourier's and Fick's laws, *Case Studies in Thermal Engineering*, Vol. 26, 2021, pp. 101186, DOI: 10.1016/j.csite.2021.101186.

[24] A. Dawar, Z. Shah, H.M. Alshehri, S. Islam, P. Kumam, Magnetized and non-magnetized Casson fluid flow with gyrotactic microorganisms over a stratified stretching cylinder, *Scientific Reports*, Vol.11,2021, pp. 16376, DOI: 10.1038/s41598-021-95878-8.

[25] N.A. Shah, A. Ebaid, T. Oreyeni, S.J. Yook, MHD and porous effects on free convection flow of viscous fluid between vertical parallel plates: advance thermal analysis, *Waves in Random and Complex Media*, DOI: 0.1080/17455030.2023.2186717.

[26] G. F. Umbricht, D. Rubio, Optimal Estimation of Thermal Diffusivity in a Thermal Energy Transfer Problem with Heat Generation Convection Dissipation and Lateral Heat Flow, *WSEAS Transactions on Fluid Mechanics*, Vol.16, 2021, pp. 222-231, https://doi.org/10.37394/232013.2021.16.21.

[27] M.H. Hamdan, Effects of Physical Coordinate Clustering on Boundary Vorticity Approximations in von Mises Coordinates, *WSEAS Transactions on Fluid Mechanics*, Vol.16, 2021, pp. 201-213, https://doi.org/10.37394/232013.2021.16.19.

[28] U. Farooq, H. Waqas, S.E. Alhazmi, A. Alhushaybari, M. Imran, R. Sadat, T. Muhammad, M.R. Ali, Numerical treatment of casson nanofluid bioconvectional flow with heat transfer due to stretching cylinder/plate: variable physical properties, *Arabian Journal of Chemistry*, Vol.16, No. 4, 2023, https://doi.org/10.1016/j.arabjc.2023.104589

[29] E. Sangeetha, P. De, Bioconvective casson nanofluid flow towards stagnation point in non-darcy porous medium with buoyancy effects, chemical reaction, and thermal radiation, *Heat Transfer*, Vol.52, No. 2, 2022, pp. 1529-1551. https://doi.org/10.1002/htj.22753

[30] R. Arpitha, N.N. Kumar, D. Srikanth, Bioconvective squeezing flow of chemically reacting casson nanofluid between two parallel plates, *Iranian Journal of Science and Technology, Transaction of Mechanical Engineerng,* Vol. 47, 2023, pp. 1615-1632

[31] M. Jawad, A. Saeed, A. Khan, S. Islam, NHD bioconvection darcy-Forchheimer flow of casson nanofluid over a rotating disk with entropy optimization, *Heat Transfer*, Vol.50, No. 3, 2020, pp. 2168-2196, https://doi.org/10.1002/htj.21973.

[32] N.A. Shah, T. Oreyeni, R. Shah, B. Salah and J.D. Chung, Brownian motion and thermophoretic diffusion effects on the dynamics of MHD upper convected Maxwell nanofluid flow past a vertical surface, *Physica Scripta*, Vol.96, pp. 125722, DOI: 10.1088/1402-4896/ac36ea.

[33] K. Al-Khaled, S.U. Khan, Thermal aspect of casson nanoliquid with gyrotactic microorganisms, temperature-dependent viscosity, and variable thermal conductivity: bio-technology and thermal application. *Inventions*, Vol. 5, No. 3, 2020, https://doi.org/10.3390/inventions5030039.

[34] S.A. Lone, MD Shamshuddin, S. Shahab, S. Iftikhar, A. Saeed, A. M. Galal, Computational analysis of MHD driven bioconvective flow of hybrid casson nanofluid past a permeable exponential stretching sheet with thermophoresis and Brownian motion effects, *Journal of Magnetism and Magnetic Materials*, Vol. 580, 2023, https://doi.org/10.1016/j.jmmm.2023.170959.

[35] H. Sharif, M. Hussain, M.A. Khadimallah, M.N. Naeem, H. Ayed, A. Tounsi, Impact in bioconvection MHD casson nanofluid flow across darcy-Forchheimer medium due to nonlinear stretching surface, *Smart Structures and Sytems*, Vol.28, No. 6, 2021, pp. 791-798, https://doi.org.190.12989/sss.2021.28.6.791.

[36] A.O. Oyem, W.N. Mutuku, A.S. Oke, Variability effects on MHD for Blasius and Sakiadis flows in the presence of Dufour and Soret about a flat plate, *Engineering Report*, e12249, 2020, pp. 1-15. https://doi.org/10.1002/eng2.12249.

[37] I.S. Oyelakin, S. Mondal, P. Sibanda, Nonlinear radiation in bioconvective casson nanofluid flow, *International Journal of Applied and Computational Mathematics*, Vol.5, No. 5, 2019, pp. 1-20, https://doi.org/101007/s40819-019-0705-0.

[38] A.S. Oke, B.A. Juma, A.O. Oyem, Hydromagnetic flow of Casson fluid carrying CNT and graphene nanoparticles in armory production, *WSEAS Transactions on Fluid Mechanics*, Vol.18, 2023, pp. 123-134. https://doi.org/10.37394/232013.2023.18.13.

Contribution of Individual Authors to the Creation of a Scientific Article (Ghostwriting Policy)

The authors equally contributed to the present research, at all stages from the formulation of the problem to the final findings and solution.

Sources of Funding for Research Presented in a Scientific Article or Scientific Article Itself

No funding was received for conducting this study.

Conflict of Interest

The authors have no conflicts of interest to declare that are relevant to the content of this article.

APPENDIX

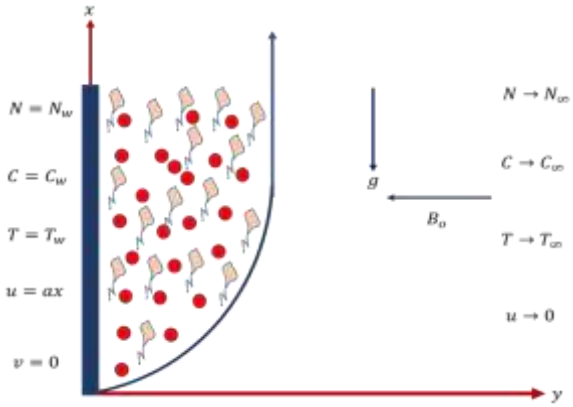

Fig. 1: Schematic diagram of the problem

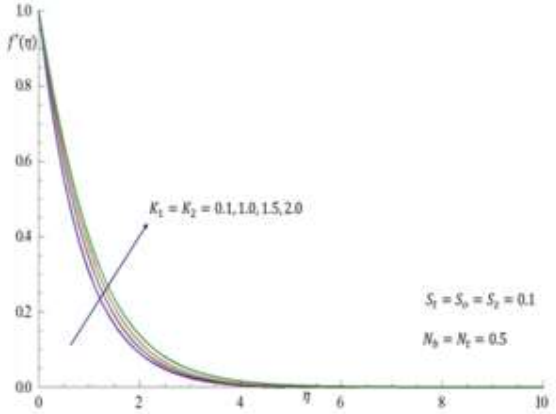

Fig. 2: Effects of K_1 and K_2 on velocity profiles

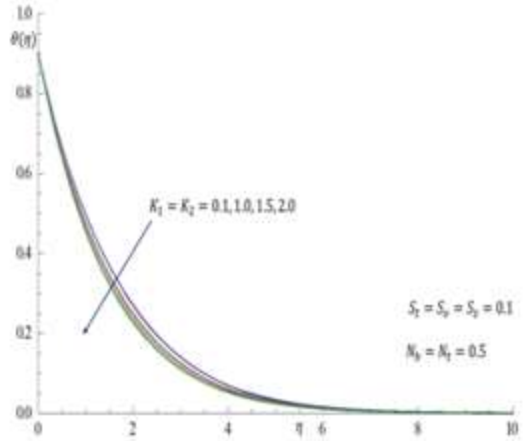

Fig. 3: Effects of K_1 & K_2 on temperature

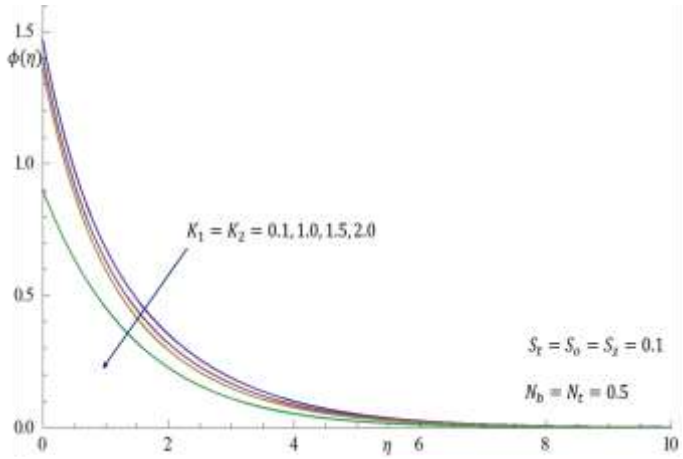

Fig. 4: Contribution of K_1 and K_2 on concentration of nanoparticles profile

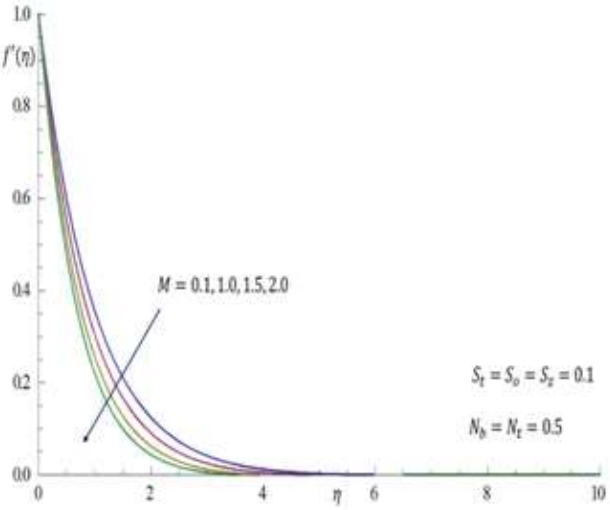

Fig. 5: Contribution of M on velocity profile

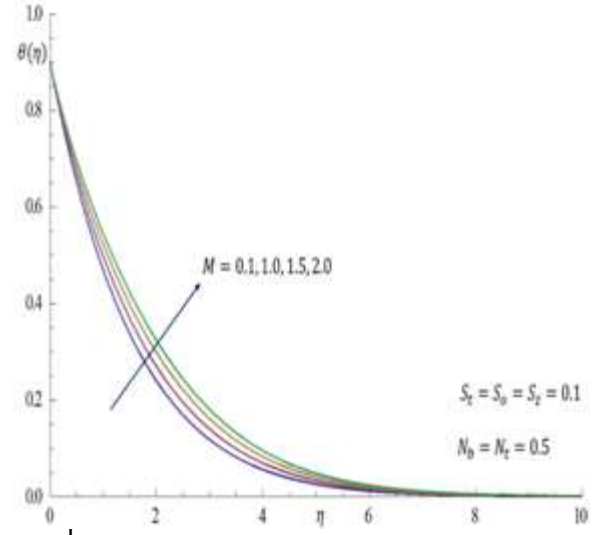

Fig. 6: Contribution of M on temperature profile

References

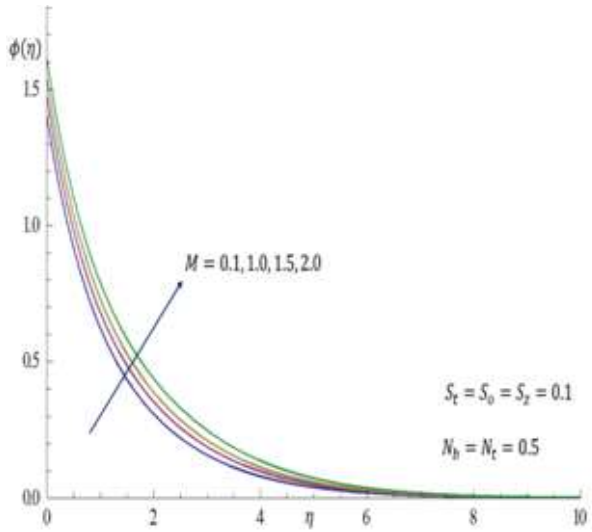

Fig. 7: Contribution of M on concentration of motile microorganism profile

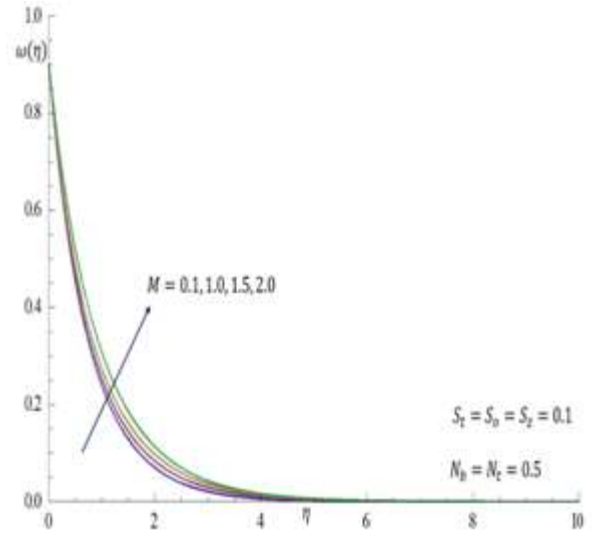

Fig. 8: Contribution of M on density of nanoparticles profile

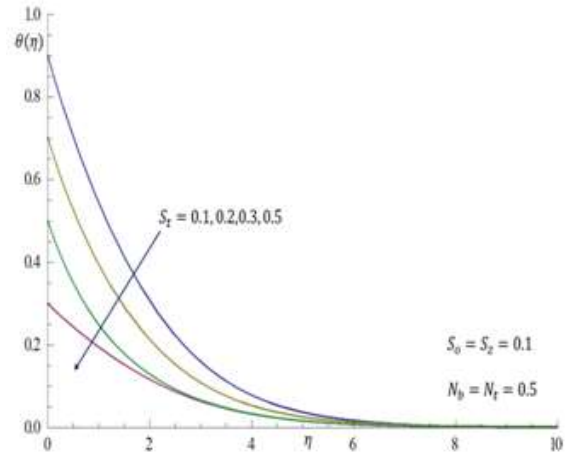

Fig. 9: Contribution of S_t on temperature profile

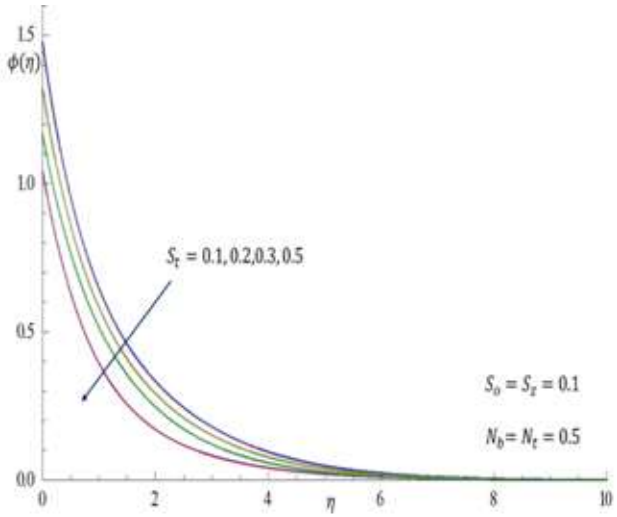

Fig. 10: Contribution of S_t on concentration of nanoparticles profile

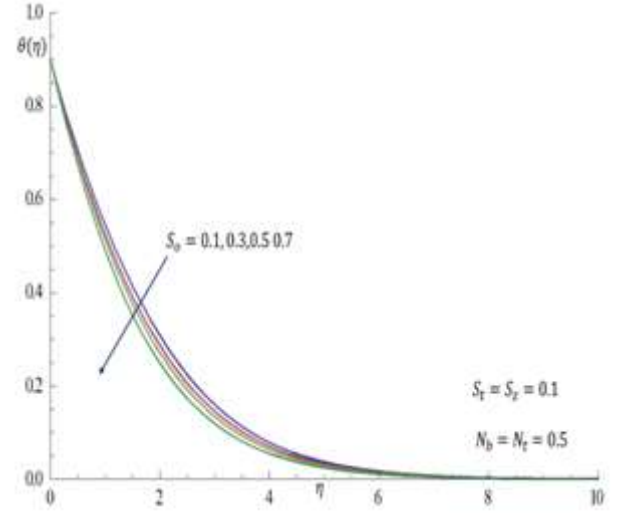

Fig. 11: Contribution of S_o on temperature of nanoparticles profiles

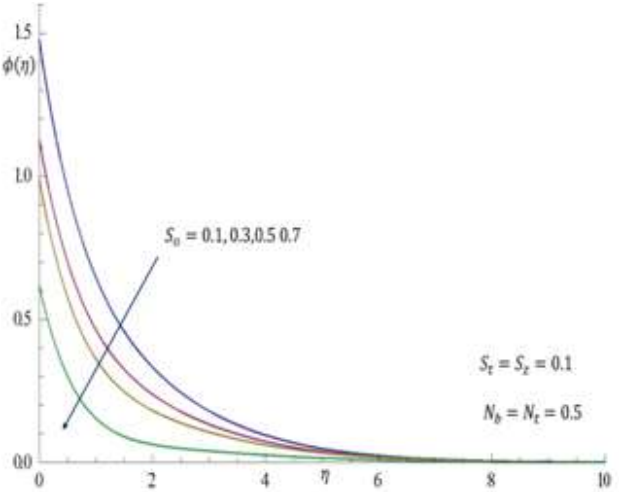

Fig. 12: Contribution of S_o on concentration Profiles

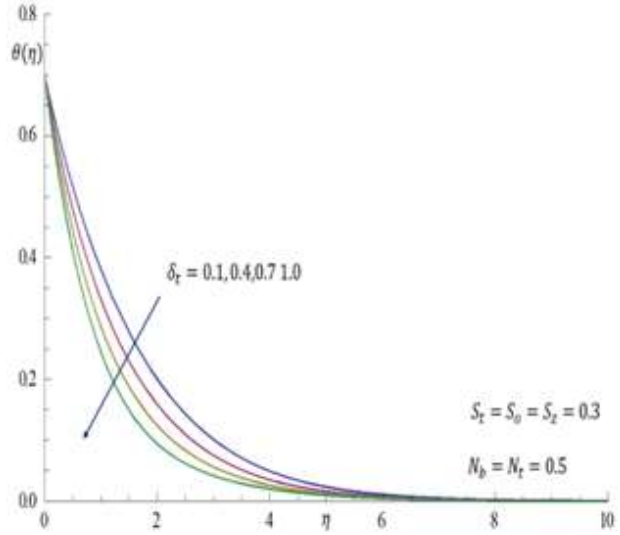

Fig. 13: Contribution of δ_t on temperature of nanoparticles profiles

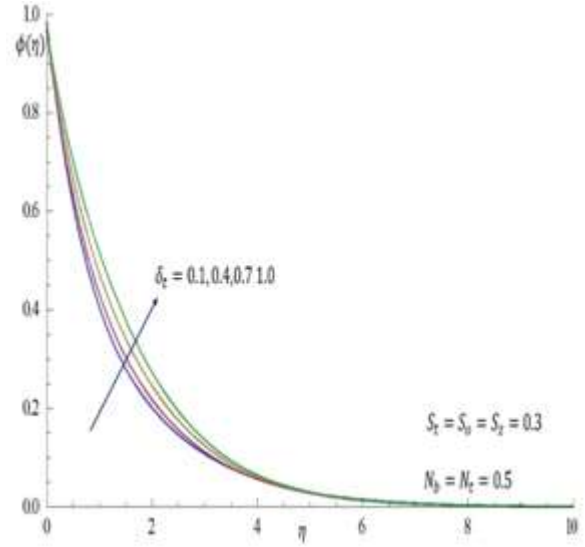

Fig. 14: Contribution of δ_t concentration profiles

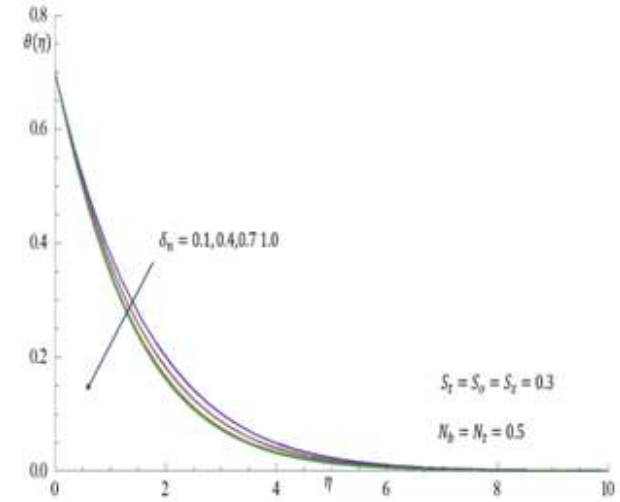

Fig. 15: Contribution of δ_n on temperature of nanoparticles profiles

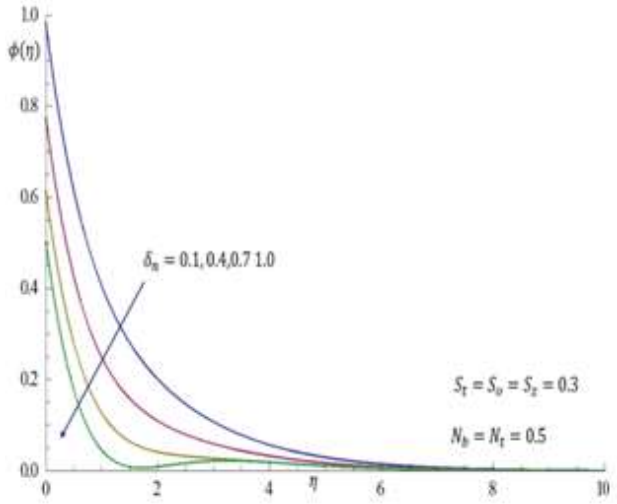

Fig. 16: Contribution of δ_n concentration profiles

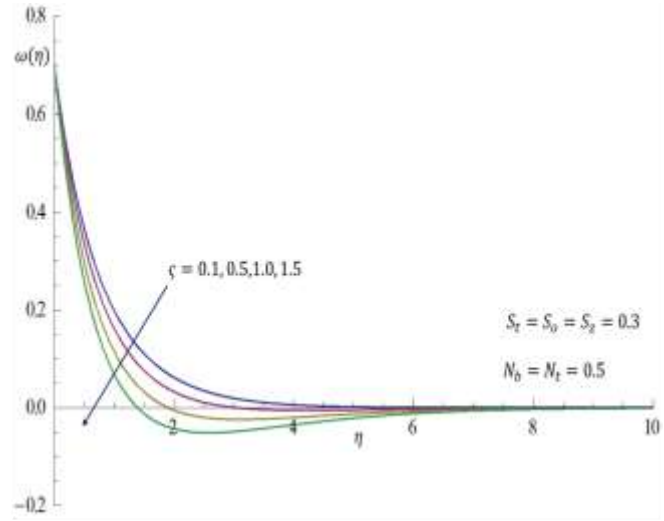

Fig. 17: Contribution of ς on density of motile micro-organisms profile

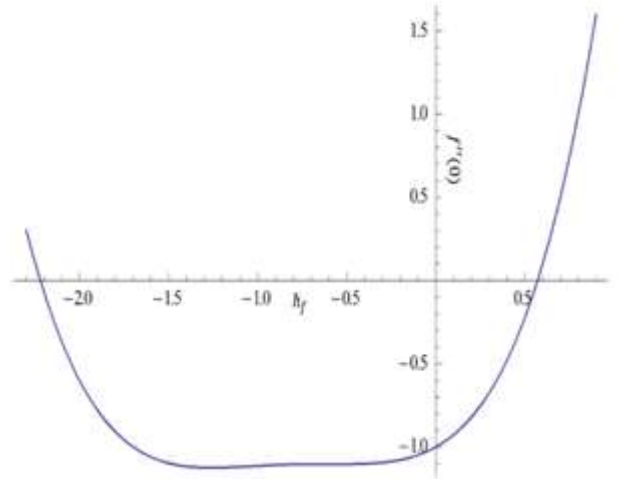

Fig. 18: $\hbar$-curve of $f''(0)$ obtained at 10th order of approximation

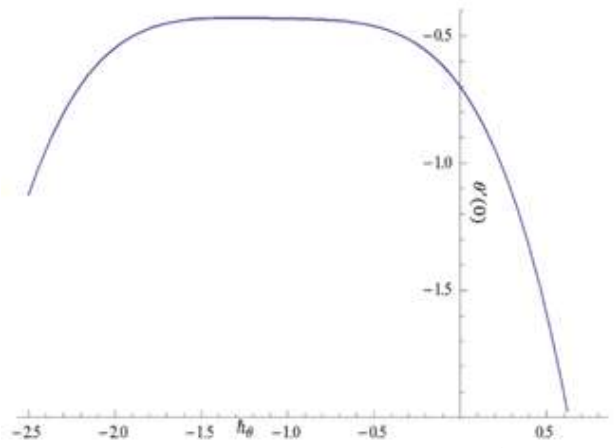

Fig. 19: $\hbar$-curve of $\theta'(0)$ obtained at 10th order of approximation

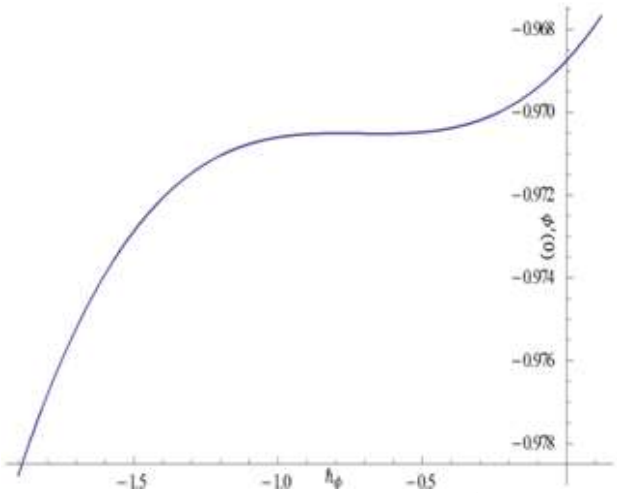

Fig. 20: $\hbar$-curve of $\phi'(0)$ obtained at 10th order of approximation

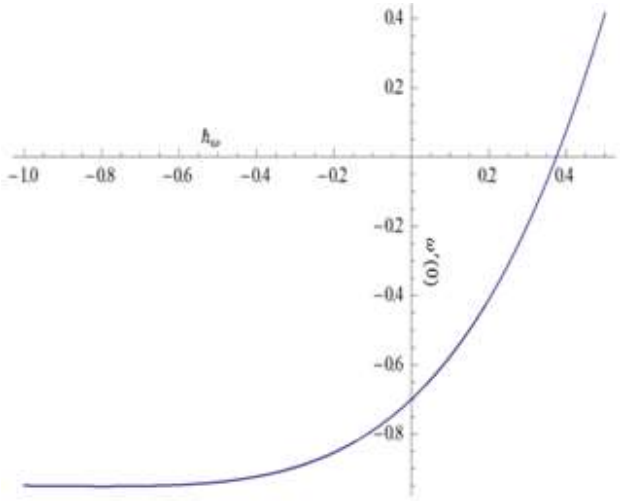

Fig. 21: $\hbar$-curve of $\omega'(0)$ obtained at 10th order of approximation

Table 1. Numerical values of skin friction coefficients and reduced Nusselt number for various values of N_b

N_b	N_t	$-f''(0)$	$-\theta'(0)$
0.1	0.2	0.8322	1.0970
0.3	0.2	1.1644	1.1338
0.5	0.2	0.6619	1.1429
0.7	0.2	0.7065	1.1445

Table 2. Numerical values of skin friction coefficients and reduced Nusselt number for various values of N_t

N_t	N_b	$-f''(0)$	$-\theta'(0)$
0.1	0.5	0.8322	1.0970
0.3	0.5	1.1644	1.1338
0.5	0.5	0.6619	1.1429
0.7	0.5	0.7065	1.1445